Comparison of Coal-Derived and Petroleum Asphaltenes by 13C Nuclear Magnetic Resonance, DEPT, and XRS

ARTICLE *in* ENERGY & FUELS · JUNE 2011

Impact Factor: 2.79 · DOI: 10.1021/ef2003443

6 AUTHORS, INCLUDING:

John C Edwards
Independent Researcher
74 PUBLICATIONS **919** CITATIONS
SEE PROFILE

Andrew E Pomerantz
Schlumberger Limited
81 PUBLICATIONS **1,283** CITATIONS
SEE PROFILE

Oliver C Mullins
Schlumberger Limited
244 PUBLICATIONS **5,948** CITATIONS
SEE PROFILE

Koyo Norinaga
Kyushu University
96 PUBLICATIONS **1,220** CITATIONS
SEE PROFILE

energy&fuels

ARTICLE

pubs.acs.org/EF

Comparison of Coal-Derived and Petroleum Asphaltenes by ^{13}C Nuclear Magnetic Resonance, DEPT, and XRS

A. Ballard Andrews,*[,†] John C. Edwards,[‡] Andrew E. Pomerantz,[†] Oliver C. Mullins,[†] Dennis Nordlund,[§] and Koyo Norinaga[∥]

[†]Schlumberger-Doll Research, Cambridge, Massachusetts 02139, United States

[‡]Process NMR Associates, Danbury, Connecticut 06810, United States

[§]Stanford Synchrotron Radiation Lightsource, SLAC National Accelerator Laboratory, Menlo Park, California 94025, United States

[∥]Hokkaido University, Sapporo, Japan

ABSTRACT: The molecular architecture of asphaltenes is still a matter of debate. Some literature reports provide evidence that the contrast of petroleum asphaltenes versus coal-derived asphaltenes is useful for understanding the governing principles of asphaltene identity. Coal-derived asphaltenes provide an excellent test for understanding the relationship of asphaltene molecular architecture with asphaltene properties. Diffusion measurements have shown that coal-derived asphaltenes are half the size of many crude oil asphaltenes, but there are relatively few studies comparing coal-derived and petroleum asphaltenes using liquid state ^{13}C NMR. ^{13}C NMR confirms that the molecular sizes of these coal-derived asphaltenes are smaller than virgin petroleum asphaltenes. DEPT-45 experiments were performed in order to determine the relative amount of nonprotonated and protonated carbon in the aromatic region of the spectrum. In contrast to previous NMR work on asphaltenes that ignored interior bridgehead carbon, we show this is an important component of asphaltenes and that correctly accounting for this carbon enables proper determination of the number of fused rings. XRS data supports interpreting the NMR data with a model that weighs circularly condensed structures more heavily than linearly condensed structures. Significantly more carbon exists in chains at least 9 carbons long in petroleum asphaltenes ($\geq$7%) compared to coal-derived asphaltenes ($\geq$1%).

INTRODUCTION

As a result of numerous studies, there has been a gradual convergence on several fundamental properties of asphaltenes.[1] Asphaltene molecular weight is a less controversial subject than it was a decade ago. Four different diffusion measurements have been employed to examine asphaltene molecular size, and by implication asphaltene molecular weight. Time resolved fluorescence depolarization (TRFD) has been used to measure the rotational diffusion constants of asphaltenes from petroleum,[2] coals,[3] and solubility subfractions of petroleum asphaltenes[4] The TRFD results show that (1) asphaltenes are relatively small in molecular size and (2) asphaltenes consist of molecules primarily with one fused ring system per molecule. Taylor dispersion diffusion measurements, which relied on optical absorption measurements to determine the translational diffusion constant of a coal-derived (CD-) asphaltene (the same sample as the TRFD study), found excellent agreement with the TRFD results.[5] NMR pulsed field gradient measurements were employed on petroleum (P-) asphaltenes and again obtained reasonable agreement with the TRFD studies for the same samples.[6] Fluorescence correlation spectroscopy (FCS) has found that the size of P-asphaltenes from different source crudes is remarkably consistent.[7,9] Asphaltene diffusion times have been compared with known polycyclic aromatic hydrocarbon (PAH) model compounds and found to be similar. The conclusion of all asphaltene diffusion measurements in general and FCS results in particular is that asphaltene molecules are small.

Boduszynski published field ionization mass spectral results that concluded the bulk of asphaltenes are under a kilodalton.[10] These results, which are in good agreement with the diffusion measurements, were somewhat discounted with the general complaint that (1) fragmentation "must" be occurring and (2) the heaviest species are not being desorbed. In recent years there has been extensive use of electrospray ionization (ESI), a technique that is known to be quite soft; it does not result in fragmentation. Fenn and others have made use of electrospray ionization Fourier-transform ion cyclotron resonance mass spectroscopy (FT-ICR MS) on crude oils[11] and asphaltenes[12,13] without detecting "large" asphaltene molecules. Laser desorption ionization (LDI) at low laser power and low surface asphaltene concentration are consistent with these results.[14] L2MS experiments show independence of measured asphaltene molecular weight on IR laser power, UV laser power, or laser pulse timing.[14−16]

The conclusion that emerges from the sum total of these studies is that asphaltene molecular weight is roughly 750 Da with 500−1000 Da full width at half-maximum (fwhm), The second primary result of the diffusion measurements (TRFD) is that there is one or perhaps two PAHs per molecule, a result which has also been controversial. There is recent support for this finding from single molecule decomposition studies independent of whether fragmentation occurs by photons,[17] helium atom

Received: March 4, 2011
Revised: May 26, 2011

collision,[18] or electron impact.[19] Additionally, an examination of PAHs coupled with spectral analysis of asphaltenes supports this finding.[20] Also note that a seven-ring PAH with ~50% alkane carbon and a heteroatom or two yields a mass of ~750 Da. Thus if seven-ring PAHs are the most probable, as claimed,[2−4,17] then a single PAH per molecule is exactly consistent with the now known molecular weights of asphaltenes. Indeed, this molecular architecture is consistent with and largely demanded by the very high degree of alignment of asphaltenes in Langmuir−Blodgett films. Sum frequency generation spectroscopy measurements (SFG) shows that in these films, the asphaltene PAH is parallel to the interface while the asphaltene alkanes are perpendicular to the interface.[21]

CD-asphaltenes have been shown to be half the size of many crude oil asphaltenes by TRFD,[3,4] FCS,[7−9] LDI,[14] and L2MS,[15] but there are relatively few studies comparing CD-asphaltenes and P-asphaltenes using liquid state ^{13}C NMR. CD-asphaltenes provide an excellent test for understanding the relationship of asphaltene molecular architecture with asphaltene properties.[3] First, CD-asphaltenes are very low mass with a ~350 Da average. There are no ambiguities concerning the sensitivity of mass spectral techniques or diffusion techniques to probe this size. Numerous studies on P-asphaltenes prove all these techniques can at least see twice this molecular weight. In addition, the number of combinations of molecular moieties greatly diminishes when the total weight is only 350 Da in comparison with 750 Da. Thus, creating plausible coal-derived asphaltene molecular models is much more constrained than for P-asphaltenes because of their very small size. In addition, CD- asphaltenes have very little alkane carbon removing further complexity. The coal-derived source material is deficient of hydrogen and alkane carbon in comparison to petroleum alkanes. Indeed, ^{13}C NMR on a CD-asphaltene showed that the CD-asphaltene has a much higher fraction of aromatic carbon than the P-asphaltene.[3] The process to obtain these CD-asphaltenes is as follows: coals are liquefied in a hydrogenation process, the coal liquids are distilled, and the resid is extracted to obtain asphaltenes. In this process, almost all oxygen is lost and pendant alkanes are also susceptible to cracking. The P-asphaltenes are generally used without any chemical processing (virgin petroleum asphaltenes), but petroleum resid asphaltenes can also be used for analysis.[22]

Three CD-asphaltenes were prepared each from the resid of a vacuum distillation of the corresponding liquefaction fraction from a particular coal. These coal-derived samples are characterized by ^{13}C NMR, and ^{1}H−^{13}C DEPT (distortionless enhancement by polarization transfer) methods to provide robust analysis of key molecular structure issues, particularly the saturate to aromatic carbon ratio. Our approach is to utilize a method whereby only ^{13}C NMR data are required to obtain the functional carbon chemistry and the calculated average cluster parameters describing the dissolved petroleum material. Throughout the manuscript we will use the term "cluster" as shorthand for "average aromatic cluster", a common parlance in the ^{13}C NMR literature. "Cluster size" (designated by C in the text and tables) refers to the number of aromatic carbon atoms in a PAH ring system where the rings are connected through aromatic bridgehead carbon atoms (carbons shared by two or more rings). The total number of carbon atoms in a cluster also includes aliphatic carbons.

The calculation of average cluster parameters is a liquid-state NMR version of the solid-state ^{13}C NMR method developed by Solum and Pugmire[23] that has become the standard processing procedure for ^{13}C NMR of carbonaceous solids (coal, soot, combustion deposits, kerogen, char, asphaltenes, etc.).[23−28] It is argued here that not utilizing DEPT NMR leads to large deviations in the calculation of accurate ^{13}C NMR parameters. Researchers in relatively recent studies[29−32] have not utilized advanced NMR techniques to separately quantify the protonated and nonprotonated aromatic carbons in the 124−129.5 ppm region of the spectrum. Comparison of the quantitative ^{13}C NMR (which observes all carbons) together with the DEPT45 experimental results (which observes only protonated carbons) provides a consistent methodology to allow this separate quantification to be performed.

2. EXPERIMENTAL SECTION

2.1. Sample Preparation. Three different CD-asphaltenes were studied, two from Indonesia, Tanito Harum (TH) and Adaro (AD), and one from the U.S., Wyoming (WY). They originated from three different sub-bituminous coals. These coals were liquefied, distilled, and the distillation resid was then extracted to obtain CD-asphaltenes. Two P-asphaltenes were studied with NMR (BG5, UG8). The Adaro coal liquefaction residue was obtained in the NEDOL 150 ton/day pilot plant (PP) which was operated during 1996−1998 at Kashima City, Ibaraki, Japan.[33] The typical liquefaction conditions were temperature 450−465 °C, pressure 16.8 MPa (in part from added H_2), gas-to-feed slurry ratio 0.7 N m^3/kg, and coal concentration in feed slurry 40 wt %. The liquefaction residue was obtained from the resid in the vacuum distillation column where the liquefaction products were separated into four fractions, i.e., the light oil fraction with the boiling point below 220 °C, the medium oil fraction with the boiling point ranging from 220 to 350 °C, the heavy oil fraction with the boiling point ranging from 350 to 538 °C, and the liquefaction residue.

The liquefaction residues from Tanito Harum and Wyoming coals were obtained in the 1 t/d process supporting unit (PSU) constructed for the support studies on the operations of the PP.[34] The operating conditions and the process flow of the PSU are similar to those of the PP. The solid residues from distillation of the coal extracts were pulverized to pass through a 60-mesh screen, and dried for 2 h under vacuum at 110 °C before use. The asphaltene fraction, which is toluene soluble and *n*-hexane insoluble, and the resin fraction, which is the *n*-hexane soluble component, were obtained with the Soxhlet extraction technique. The yields and the elemental compositions of the asphaltene and oil samples are given in Table 1.

Asphaltenes were extracted from a black oil (UG8) using standard procedures. Briefly, an oil sample was diluted 1:40 in *n*-heptane and stirred for 24 h. Asphaltenes were extracted from the solution by vacuum filtration through a nylon filter with 1.2-μm pores and were washed with additional *n*-heptane until the wash solvent was colorless. The extracted asphaltenes were then resuspended in a small volume of toluene. This solution was diluted 1:40 in *n*-heptane, and the asphaltenes were extracted as before. Finally, the asphaltenes were washed by extensive Soxhlet extraction in *n*-heptane.

2.2. NMR Methods. ^{13}C NMR spectra were obtained on a Varian Unity-300 Spectrometer operating at a resonance frequency of 75.427 MHz with a Varian 5 mm broad-band probe. ^{13}C NMR spectra were obtained with a 8 μs (π/3) pulse width, a 25 kHz spectral width, a 2 s relaxation delay, and a 0.484 s acquisition time. Quantitative ^{13}C NMR spectra were obtained utilizing inverse gated decoupling to prevent NOE signal enhancements that are related to the proton environments of carbons in the sample, and thus cause nonquantitative enhancements of highly protonated carbons (CH_2 and CH_3) over lesser protonated carbons (CH and C). As further quantitative strategy the samples are dissolved in a deuterated solvent comprising 2/1 $CDCl_3$−CrAcAc (0.05 M)/CS_2 which reduces the ^{13}C T_1 relaxation times to values of around 0.25 s allowing pulse repetition rates of around 2 s to be employed for increased signal averaging in a shorter time frame and ensuring that all carbons are observed equally, especially the internal aromatic carbons in

Table 1. Elemental Composition and Yield for Coal-Derived Asphaltenes and Petroleum-Derived Asphaltenes

		wt %, dry					
	resid yield wt %	C	H	N	S	O (by difference)	H:C atomic ratio
			coal-derived asphaltene				
Tanito Harum	24	90.56	5.59	2.11	0.1	1.64	0.74
Wyoming	25	89.41	6.04	1.43	0.13	2.99	0.81
Adaro	48	88.75	6.25	1.45	0.09	3.46	0.85
			petroleum asphaltene				
BG5		79.2	7.82	0.98	7.61	2.45	1.18
						(measured)	
UG8		81.07	7.11	1.02	8.94	1.6	1.05

pericondensed aromatics which can have very long T_1 relaxation times if paramagnetic relaxation agents are not employed.

The chemical shift ranges used for the integrations in this study are detailed in the book on NMR applied to heavy petroleum products by Boduszynski and Altgelt,[35] which is based on a large body of ^{13}C literature in the area of solid-state NMR analysis. It is common knowledge that similar chemical shifts are obtained in liquid and solid state NMR. Chapters 5 and 8 in ref 30 contain descriptions of NMR approaches and detailed ^{1}H and ^{13}C NMR chemical shift tables. The aromatic carbon shifts in ref 35 (see Table 5.5, Ch. 5), are taken from papers dealing with coal liquids[36,37] and lighter hydrocarbons.[38] Table 2 represents a summary condensation of these integration limits, however here we restrict our attention to the aromatic portion of the ^{13}C spectra. This method is applicable to any hydrocarbon, and in general NMR chemical shift ranges are identical whether one is dealing with naphtha, diesel, vacuum gas oil, or asphaltenes. However, these simple integration calculations performed on ^{13}C SPE (single pulse excitation) spectra suffer from the almost complete overlap of protonated and nonprotonated carbon signals in the 108−129.5 ppm region of the spectrum, leading to underestimation of nonprotonated carbon content that occurs using such traditional chemical shift region integrations. Note that nonprotonated carbons are sometimes referred to as quaternary carbons in ^{13}C NMR literature, however to avoid confusion we have opted not to use the latter terminology.

To accurately determine the relative amount of nonprotonated and protonated carbon in the aromatic region of the spectrum where the signals overlap we carried out DEPT-45 experiments. DEPT is based experimentally on a proton-to-carbon polarization transfer through the C−H J-coupling. The issues with quantification in DEPT experiments are caused by two factors: (1) the fact that there is a range of J-coupling values, the J-coupling of aromatic C−H and aliphatic C−H are different by about 20 Hz, and (2) carbons with different numbers of protons attached polarize at different rates as described below:[39]

$$\mathrm{CH}: \text{Signal Intensity} = [\gamma(^{1}\mathrm{H})/\gamma(^{13}\mathrm{C})]\sin\theta$$

$$\mathrm{CH_2}: \text{Signal Intensity} = [\gamma(^{1}\mathrm{H})/\gamma(^{13}\mathrm{C})]\sin 2\theta$$

$$\mathrm{CH_3}: \text{Signal Intensity} = [3\gamma(^{1}\mathrm{H})/4\gamma(^{13}\mathrm{C})](\sin\theta + \sin 3\theta)$$

where γ is the magnetogyric ratio of the nucleus.

In practice the J coupling value differences do not play a significant role in preventing quantification, and the signal intensity behavior is understood well enough that quantitative comparisons among CH, CH_2, and CH_3 protonated carbons can be made. Many researchers have published findings in this regard.[40−49] Begon et al.[50] performed analyses similar to those described here, utilizing DEPT and QUAT pulse sequences to quantify nonprotonated aromatic carbon in a coal, coal extract, and a hydrocracked product.

Table 2. Chemical Shifts and Integration Limits for Evaluating the Aromatic and Aliphatic Contributions

carbon NMR regions	begin (ppm)	end (ppm)
phenolic C	160	150
substituted aromatic C	150	133
bridgehead aromatic C	133	129.5
bridgehead + protonated aromatic C	129.5	124
protonated/hetero aromatic C	124	108
aliphatic C	60	5

In DEPT only protonated carbons are observed and a simple ratio calculation can be performed in order to calculate the relative amount of paraffinic CH_3 to aromatic CH to obtain a quantitative ratio. This ratio is then applied to the quantitative ^{13}C NMR data obtained on the same sample to effectively subtract out the protonated aromatic carbon intensity found in the 124−129.5 ppm region of the spectrum. By comparison with these same signal intensities observed in the quantitative (SPE) experiment it is possible to quantitatively determine the amount of nonprotonated carbon present in the aromatic region of the spectrum (108−160 ppm)[40,49] and calculate all of the molecular and chemical parameters directly from the ^{13}C SPE and DEPT45 without additional assumptions. Once the bridgehead carbon content of pericondensed aromatics in the 124−129.5 ppm region is added to the bridgehead aromatic carbon of catacondensed aromatics found in the 129.5−133 ppm region it is possible to determine the mole fraction of bridgehead carbons (X_b). Once this value is know it is possible to determine the average aromatic cluster size and then calculate the remaining average molecule parameters described in the Solum and Pugmire paper[23] based on a 100 carbon description of the sample.

2.3. XRS Methods. Carbon K-edge X-ray Raman spectroscopy (XRS) experiments were performed on beamline 6-2 at Stanford Synchrotron Radiation Lightsource, using a spectrometer similar to that described previously.[51,52] Briefly, synchrotron radiation in the range 6730−6790 eV was selected using a Si (311) double crystal monochromator, resulting in a flux of 10^{12} photons/sec over a 150 × 150 μm spot size and an energy resolution of 0.5 eV full width at half-maximum. Raman scattering was collected using a high-energy-resolution multicrystal analyzer in a Rowland geometry (R = 1 m), employing 14 Si (440) analyzer crystals (100 mm in diameter) at a fixed Bragg angle of 88°. This setup selects 6460 eV photons with a resolution of ~0.35 eV and momentum transfer of $q = 2.6$ Å^{-1}. With the radius of the carbon 1s shell $r = 0.091$ Å,[53] the XRS spectrum is dominated by dipole transitions that are equivalent to the direct carbon 1s soft X-ray absorption (XAS),[54]

dx.doi.org/10.1021/ef2003443 |Energy Fuels XXXX, XXX, 000–000

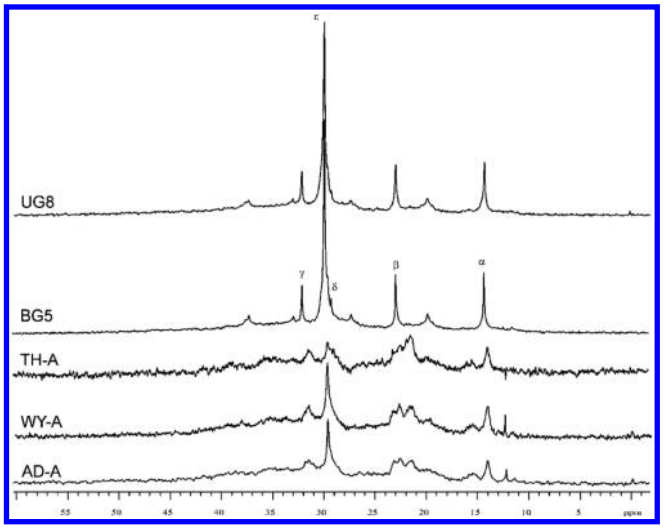

Figure 1. Aliphatic portion of the ^{13}C NMR spectra for three CD-asphaltene samples (TH-A, WY-A, AD-A) and two P-asphaltenes (BG5, UG8). Table 3 lists the aliphatic wt % obtained using chemical shifts specified in Table 2. The peaks labeled α, β, γ, δ, and ε arise from terminal carbons (α, 14 ppm), and carbons that are 1 (β, 22.7 ppm), 2 (γ, 32 ppm), 3 (δ, 29.7 ppm), and 4 (ε, 30.1 ppm) or more carbons away from the terminal carbon. The *n*-paraffin wt % is obtained by integrating these peaks.

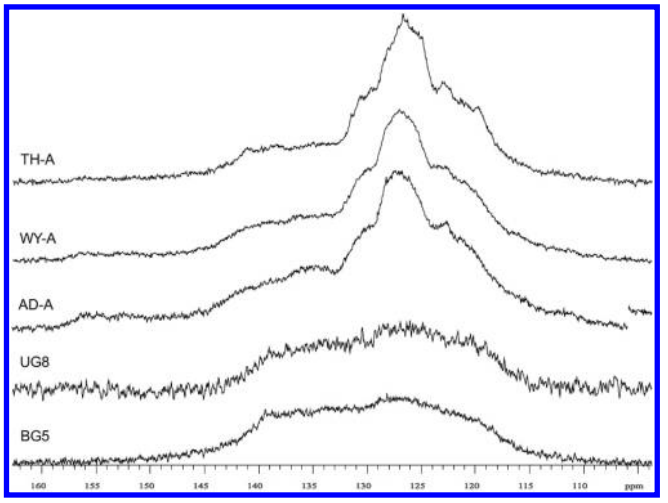

Figure 2. Aromatic portion of the ^{13}C NMR spectra for three CD-asphaltene samples (TH-A, AD-A, WY-A) and two P-asphaltenes (BG5, UG8). Table 3 lists the aromatic wt % obtained by integration using the chemical shifts specified in Table 2. The P-asphaltenes have roughly 50% aromatic carbon whereas the CD-asphaltenes are close to 80% aromatic carbon.

with XRS having the advantage of more bulk sensitivity and less complication due to thickness effects. Higher order contributions, for example to s-like states, contribute less than 10% ($qr/2 \sim 0.1 \ll 1$) to the observed XRS spectrum. Spectra were acquired by measuring the Raman scattered photons on a photon-counting single element silicon drift detector while scanning the incident photon energy over the described range, and the detected intensity was normalized at each point against the incoming photon flux measured using a He drift tube. To correct for energy drift and positioning errors, the elastic peak was measured before acquiring each spectrum, and the Raman shift is computed as the difference between the energy selected by the monochromator and the energy of the elastic peak. Finally, spectra were baseline corrected using the pre-edge region and were normalized by setting the intensity of the post-edge step to unity.

Table 3. ^{13}C NMR Results for Coal-Derived Asphaltenes: AD and TH are Indonesian Coals, WY is a U.S. Coal, and BG5 and UG8 are Both Middle Eastern Petroleum Asphaltenes

carbon NMR parameter	AD	TH	WY	BG5	UG8
carbon aromaticity %	76.7	88.2	82.2	46.7	50.1
carbon aliphaticity %	23.3	11.8	17.8	53.3	49.9
phenolic aromatic C%	3	1.2	2.1	0.4	0.4
substituted aromatic C%	18.8	17.3	17.8	15.6	16
bridgehead aromatic C%	33.7	47.9	42.7	22.9	28.1
protonated/hetero aromatic C %	21.1	21.9	19.6	7.8	5.6
X_b-mole fraction of bridgehead C	0.44	0.543	0.52	0.491	0.56
C - average aromatic PAH size	21.4	28.1	26.1	24.1	29.9
no. aromatic clusters per 100 carbons	3.6	2.9	3.2	1.9	1.7
substitutions per cluster	5.3	5.5	5.7	8.1	9.6
average length of substitutions	1.2	0.7	1.0	3.5	3.1
carbon in linear paraffins %	2.6	1.9	3.5	16.5	14.6
carbon in epsilon chains %	1.2	0.4	1.2	7.9	7.0
carbon atoms per cluster	27.9	31.86	31.75	51.61	59.68
sulfur atoms per cluster	0.0	0.0	0.0	1.9	2.5
nitrogen atoms per cluster	0.4	0.7	0.4	0.6	0.6
oxygen atoms per cluster	0.8	0.5	0.8	1.2	0.9
average cluster weight	372	419	416	776	880

3. RESULTS AND DISCUSSION

Previously, it was noted a CD-asphaltene had much less alkane carbon than petroleum asphaltene, in concert with the much smaller alkane content of the source materials, coal and crude oil, respectively.[3] Moreover, resid asphaltenes, having undergone some cracking of peripheral alkane, are intermediate between virgin P-asphaltenes and CD-asphaltenes.[22] An argument has been advanced that two primary molecular determinants control asphaltene solubility and must be balanced to give toluene solubility and heptane insolubility. Steric repulsion of alkane substituents must balance attractive van der Waals forces associated with PAHs. Steric repulsion of alkanes is known from basic chemistry principles even with regard to strongly impacting melting points of alkyl aromatics.[3] The direct impact of alkane peripheral substituents on PAH solubility is known in the dye industry as has been shown for alkyl substituted hetero-PAHs relevant to asphaltenes.[4] Moreover, the direct impact of disruption of order due to alkane substituents has been shown by transmission electron microscopy on model alkyl-substituted PAHs and P-asphaltenes and CD-asphaltenes.[55] The attractive effect of larger PAHs is well-known, e.g., in the widespread use of decolorizing carbon trapping larger undesired reaction products. If net molecular repulsion is too large, the molecules become *n*-heptane soluble, and thus not asphaltenes, whereas if net molecular attraction is too large, toluene insolubility results. For example, in thermal decomposition, the alkanes are cracked off the rings, which reduces repulsion while the PAH attraction remains; the net effect is coke generation. Moreover, the cracking of alkanes off resins decreases solubility and this thermally modified fraction becomes asphaltenes of smaller molecular size.[22]

dx.doi.org/10.1021/ef2003443 |*Energy Fuels* XXXX, XXX, 000–000

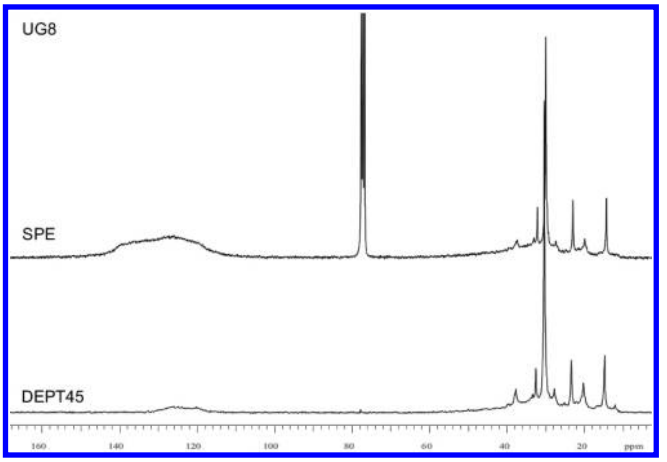

Figure 3. Comparison of the normal quantitative ^{13}C SPE and DEPT45 spectra for the P-asphaltene sample UG8. Quantitative SPE underestimates the bridgehead carbon by 50−90%.

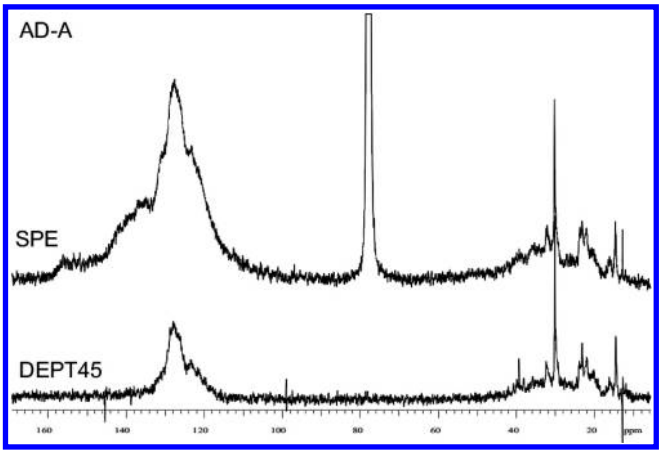

Figure 4. Comparison of the normal quantitative ^{13}C SPE and DEPT45 spectra for the CD-asphaltene sample AD-A. Quantitative SPE underestimates the bridgehead carbon by 50−90%.

We now explore the primary molecular structure differences. Table 1 shows the large difference in the H:C atomic ratio of all CD-asphaltene samples vs the P-asphaltenes. Figures 1 and 2 compare the aliphatic and aromatic ^{13}C NMR response for the CD-asphaltene and P-asphaltene fractions. The aromatic region is more pronounced in the CD-asphaltenes, while the aliphatic region is more pronounced in the P-asphaltenes. Integration of the aromatic (Table 3, row 1) and aliphatic (Table 3, row 2) regions shows that the P-asphaltene has ∼50% aromatic carbon while the CD-asphaltenes average ∼80% aromatic carbon. The SPE data are integrated to obtain the phenolic (Table 3, row 3) and alkyl-substituted (Table 3, row 4) percents. The relative concentrations of bridgehead aromatic (Table 3, row 5) and protonated/hetero aromatic (Table 3, row 6), carbons are derived from the normalization of the relative signal intensities of paraffinic CH_3 (0−20 ppm) and aromatic CH in ^{13}C DEPT45 with those observed in the ^{13}C SPE spectra, as described in the Experimental section. Figure 3 (P-asphaltene) and Figure 4 (CD-asphaltene) compare the SPE and DEPT45 ^{13}C spectral response.

To estimate the average aromatic cluster size we follow the method developed in ref 23. The ratio of bridgehead carbon to total aromatic carbon gives the mole fraction of bridgehead carbon χ_b (Table 3, row 7). Figure 5 shows a plot of χ_b vs the number of carbons per aromatic cluster C (Figure 6 in ref 23) for linear (dashed lower) and circular (dashed upper) concatenation. The number of aromatic carbons per cluster C is calculated from a weighted average of these two limits (eq 18 in ref 23).

$$\chi_b = \frac{1 - tanh((C - 19.57)/4.15)}{2}\chi_b' + \frac{1 + tanh((C - 19.57)/4.15)}{2}\chi_b'' \quad (1)$$

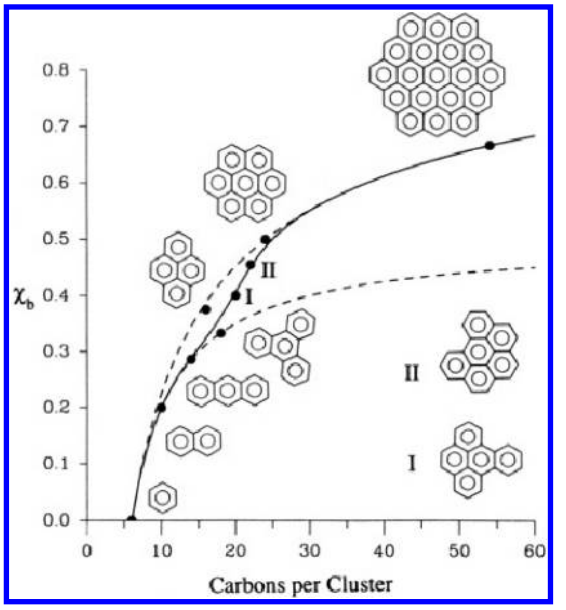

Figure 5. Plot showing the mole fraction of bridgehead carbons vs the number of carbons per aromatic cluster. The dashed curves are the two limits of circular (upper) and linear (lower) concatenation. The solid line is a best fit of the dependence of χ_b on C (for further explanation see ref 23; reproduced with permission of the publisher).

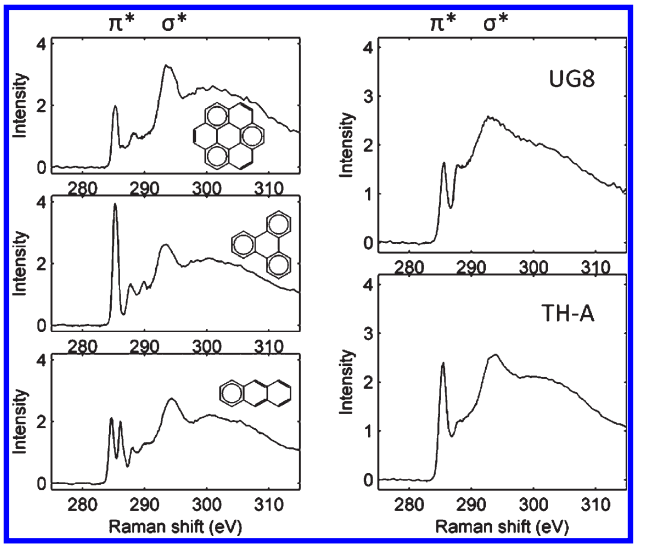

Figure 6. Carbon K-edge XRS spectra of three model compounds and UG8 and TH-A asphaltenes. 1s-π^* and 1s-σ^* transitions are observed as indicated.

dx.doi.org/10.1021/ef2003443 |*Energy Fuels* XXXX, XXX, 000–000

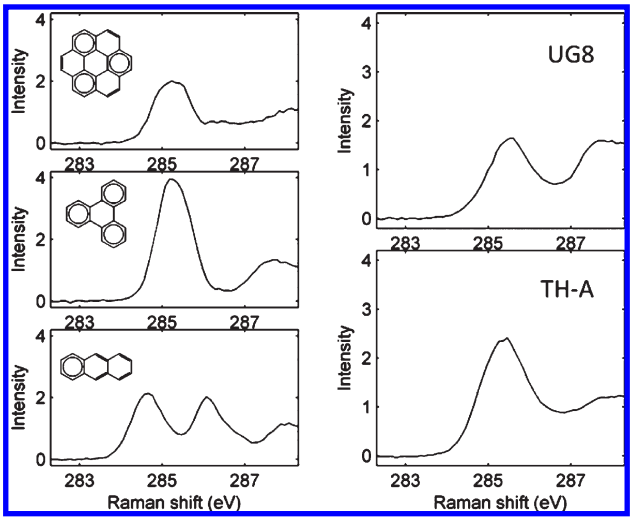

Figure 7. Zoom in of the 1s-π^* region of the XRS spectra. UG8 and TH-A asphaltenes show predominately a single 1s-π^* peak, indicating that asphaltenes may be dominated by model compounds similar to coronene (top left) or triphenylene (middle left), which display similar spectra. Anthracene (bottom left) produces two 1s-π^* peaks, so compounds similar to anthracene cannot dominate asphaltenes.

where $\chi'_b = 1/3 - 3/C$ is the mole fraction of bridgehead carbon for linear concatenation and $\chi_b = 1 - (6/C)^{1/2}$ is the mole fraction of bridgehead carbon for circular concatenation.[23] The large χ_b values imply that circular concatenation predominates, and the calculated C values are shown in row 8 of Table 3.

Both P-asphaltenes and CD-asphaltenes are more likely to be dominated by circularly condensed species than by linearly condensed species, as demonstrated in Figures 6 and 7. Figures 6 and 7 show the carbon K-edge X-ray Raman spectrum of 3 model compounds (coronene, triphenylene, and anthracene), UG8 asphaltene, and TH-A asphaltene. Figure 6 shows the pre-edge, edge, and post-edge regions, where 1s-π^* transitions and a 1s-σ^* transitions are observed as indicated on the plot. Figure 7 presents the same data but zooms in 1s-π^* transition, which is sensitive to the geometry of fused aromatic rings.[51,52,54,56] These spectra are analyzed in terms of the Clar model of aromatic clusters.[57] Briefly, the Clar model states that two types of bonds dominate aromatic clusters: aromatic sextets (drawn as circles) and isolated double bonds (drawn as double bonds). XRS can resolve these two bonding environments, with compounds dominated by aromatic sextets such as coronene (top spectrum, 18 carbons in aromatic sextets, 6 carbons in isolated double bonds) and triphenylene (middle spectrum, 18 carbons in aromatic sextets, 0 carbons in isolated double bonds) resulting in a single 1s-π^* peak, while compounds with a larger fraction of isolated double bonds such as anthracene (bottom spectrum, 6 carbons in aromatic sextets, 8 carbons in isolated double bonds) result in two 1s-π^* peaks. Both P-asphaltenes and CD-asphaltenes present a single 1s-π^* peak, suggesting that both asphaltenes are dominated by aromatic ring systems containing mostly aromatic sextets. According to the Clar model, circularly condensed species are always dominated by aromatic sextets, while linearly condensed species can be dominated by aromatic sextets if they contain branched-line (i.e., triphenylene) or zigzag-line (i.e., phenanthrene) structures but have a large fraction of isolated double bonds if they contain straight-line (i.e., anthracene) structures. Because all circularly condensed structures potentially dominate asphaltenes while certain linearly condensed structures (straight-line structures) can be excluded from dominating asphaltenes, the NMR data are most appropriately interpreted by a model weighting circularly condensed structures more heavily than linearly condensed structures.

The average carbon number per PAH decreases from P-asphaltenes to CD-asphaltenes, with roughly only one additional ring per cluster for the P-asphaltenes, compared to the CD-asphaltenes. NMR finds that CD-asphaltenes are somewhat smaller than P-asphaltenes (on average), but not significantly. This could be because P-asphaltenes are known to contain hetero atoms in aromatic rings, and S and N would not be counted (Table 1). Also, hydrogen extraction measurements on P-asphaltenes indicate 2−3 alicyclic rings per PAH,[58] which NMR would count as aliphatic and not factor into the ring size calculations.

From the literature it appears that many research groups are grossly underestimating the amount of bridgehead aromatic carbon by ignoring this issue. For example, in the studies by Sheremata et al.,[29] Michon et al.,[30] and Japanwala et al.,[31] the internal bridgehead aromatics found in the 124−129.5 ppm region are completely overlooked and seemingly not brought into the calculations. This underestimation of bridgehead aromatic carbon content will lead to a lower aromatic ring size in their calculations. The chemical shift assignments utilized by these studies were criticized in a paper by Christopher et al.[32] where it was shown by quantitative work, including DEPT, that the traditional assignment of 129.5 ppm as the absolute cutoff between protonated and nonprotonated aromatic carbons was incorrect.[35] Note that the cutoff between bridgehead and alkyl-substituted aromatics at 133 ppm is from the article by Artok et al.[59]

The number of (aliphatic) substitutions per cluster (Table 3, row 10), is calculated by dividing the aliphatic substituted aromatic carbon wt % (Table 3, row 4), by the number of clusters per 100 carbons (Table 3, row 9). The average length of substitutions (Table 3, row 11), is obtained by dividing the carbon aliphaticity (Table 3, row 2), by the total number of aliphatic substitutions (Table 3, row 10), on aromatic clusters. The average chain lengths derived by this method are relatively short, but it would be misleading to conclude that aliphatic chain lengths in P-asphaltenes are narrowly distributed around 3−4 carbons long. The peaks labeled α, β, γ, δ, and ε in Figure 1 arise from terminal carbons (α, 14 ppm), and carbons that are 1 (β, 22.7 ppm), 2 (γ, 32 ppm), 3 (δ, 29.7 ppm), and 4 (ε, 30.1 ppm) or more carbons away from the terminal carbon. Integration of these peaks yields the number of carbons in linear *n*-paraffins[60] (Table 3, row 12). In coals the *n*-paraffins (2.7%) are present at low levels and are broadened, indicating that they are relatively shorter and present in a larger range of chemical configurations than the P-asphaltenes (15.6%). The remaining saturated carbon intensity includes napthenic carbon and iso-paraffins.

A more important indicator of the structural differences between P-asphaltenes and CD-asphaltenes is the significantly larger intensity of the ε carbon peak (Figure 1) in the P-asphaltenes. Epsilon carbons that resonate at 30 ppm are defined as carbons at least 4 carbons from the end of a chain, including chains ending in a methyl group, branch points, and aromatic rings.[30] Epsilon carbons exist only in chains at least 9 carbons long (4 on either side of the epsilon carbon plus the epsilon carbon itself), and the fraction of epsilon carbon (Table 3, row 13), represents a lower limit of the amount of carbon present in chains at least 9 carbons long (those chains also contain α, β, γ, δ carbons). Despite the short average chains lengths, epsilon carbons are observed in both P-asphaltenes and CD-asphaltenes:

dx.doi.org/10.1021/ef2003443 |*Energy Fuels* XXXX, XXX, 000–000

in P-asphaltenes epsilon carbons comprise 7.5% of total carbon, and in CD-asphaltenes epsilon carbons comprise only 1% of total carbon. Therefore, at least 15% of aliphatic carbon in P-asphaltenes and 6% of aliphatic carbon in CD-asphaltenes exists in chains at least 9 carbons long. The presence of aliphatic chains exceeding 9 carbons long in P-asphaltenes is consistent with previous experiments employing Ruthenium ion catalyzed oxidation,[61−63] pyrolysis,[63,64] fragmentation patterns in electron ionization mass spectrometry,[19] and gel permeation chromatography.[65] Thus while the average substitution length is short, the distribution of chain lengths is quite broad, and a significant amount of carbon is present in long chains. This also represents an important difference between CD-asphaltenes and P-asphaltenes: not only do CD-asphaltenes have less aliphatic carbon, but a smaller fraction of the aliphatic carbon is in long chains.

Table 3 rows 14−17 list the number of atoms of each element in an average cluster. For the carbon and hydrogen, the numbers are based on the measurements already discussed in Table 3. Hydrogen is counted by summing the protonated and aliphatic carbons. For the heteroatoms sulfur, nitrogen, and oxygen which are not detected in ^{13}C NMR, the numbers are calculated from the elemental concentrations given in Table 1. In Table 3 row 18 the average cluster weight of each sample is estimated (from rows 14−17) as follows: M_n = (C * 12) + (no. of protonated aromatic carbons per cluster) + (average length of aliphatic substitutions * no. of alkyl substitutions per cluster * 14) + (S per cluster * 32) + (N per cluster * 14) + (O per cluster * 16). The average M_n (Table 3, row 17) of P-asphaltene clusters (828) is twice that of the CD-asphaltenes (402) in agreement with much of the literature.[10−20] The M_n differences apparently derive mainly from the difference in the aliphatic distributions, since the aromatic ring sizes are not as dissimilar. The small molecular weight of the CD-asphaltenes coupled with their fairly large PAH (∼6 rings) and with their very small alkane fraction is consistent with the island molecular architecture. Very similar conclusions have been made regarding asphaltene derivatives in ocean water from natural processes.[66] The asphaltene derivatives in the dissolved organic matter in the oceans lack alkane due to biodegradation and are characterized by a single, large PAH (∼7 rings) per molecule.

The island molecular architecture was first found by the TRFD studies[2−4,22] and is now supported by three different types of unimolecular decomposition studies.[15−17] Indeed, these decomposition studies show that in contrast to asphaltenes, archipelago model compounds are unstable which likely explains why they are not found in crude oil. These results are consistent with the first direct measurements of molecular orientation of asphaltenes in Langmuir−Blodgett films.[21] The results herein describe why previous NMR interpretations of PAH size in asphaltenes were inconsistent with all these other results. Our results herein align the NMR interpretation with these other studies showing that the island molecular architecture predominates.

CONCLUSIONS

NMR applied to several CD-asphaltenes has shown that the indications previously found regarding differences in CD-asphaltenes versus P-asphaltenes are indeed general and robust. These substantial differences in aromatic to saturate carbon are seen to correlate very well with diffusion constants determined from FCS.[7−9] Thus there is a sharp contrast between all CD-asphaltenes versus the P-asphaltene in the ratio of aromatic to saturated carbon. Unlike the combined ^{1}H/^{13}C/elemental analysis/assumptions methods seen in some of the literature,[30] these values are derived from a single analytical technique observing the carbons directly and without making any assumptions or requiring elemental data. Whatever normalization error there may be in the DEPT to quantitative ^{13}C comparison, it is consistently present for each asphaltene sample and thus allows values to be compared from one sample to another. A broad distribution of chain lengths is observed, and P-asphaltenes have seven times as much carbon in long chains (>9 carbons) as CD-asphaltenes.

The comparison between CD-asphaltenes and P-asphaltenes offers the prospect of sorting out structure−function relationships in these materials. In particular, the central issue of the number of PAHs in asphaltene molecules can be addressed more readily in CD-asphaltenes than P-asphaltenes because the former are smaller thereby issuing very tight constraints on molecular architecture. This report helps to build a literature base of these coal-derived derived materials, a necessary step in their thorough understanding. NMR analysis of CD-asphaltenes shows that they possess relatively large PAHs (∼6 fused rings). Given their small molecular weight, it is likely that a single PAH per molecule dominates.

AUTHOR INFORMATION

Corresponding Author
*E-mail: bandrews@slb.com.

ACKNOWLEDGMENT

Portions of this research were carried out at the Stanford Synchrotron Radiation Light source, a division of SLAC National Accelerator Laboratory and an Office of Science User Facility operated for the U.S. Department of Energy Office of Science by Stanford University. We thank H. Zheng (Schlumberger) for providing the BG5 sample and Prof. B. Blumich (RWTH Aachen) for proofreading an early version of the manuscript.

REFERENCES

(1) Mullins, O. C., Sheu, E. Y., Hammami, A., Marshall, A. G., Eds. *Asphaltenes, Heavy Oils and Petroleomics*; Springer: New York, 2007.

(2) Groenzin, H.; Mullins, O. C. Molecular sizes of asphaltenes from different origin. *Energy Fuels* **2000**, *14*, 677.

(3) Buenrostro-Gonzalez, E.; Groenzin, H.; Lira-Galeana, C.; Mullins, O. C. The overriding chemical principles that define asphaltenes. *Energy Fuels* **2001**, *15*, 972.

(4) Badre, S; Goncalves, C. C.; Norinaga, K; Gustavson, G; Mullins, O. C. Molecular size and weight of asphaltene and asphaltene solubility fractions from coals, crude oils and bitumen. *Fuel* **2006**, *85*, 1.

(5) Wargadalam, V. J.; Norinaga, K.; Iino, M. Size and shape of a coal asphaltene studied by viscosity and diffusion coefficient measurements. *Fuel* **2002**, *81*, 1403.

(6) Freed, D. E. Lisitza, N. V. Sen, P. N. Song, Y.-Q. Asphaltene molecular composition and dynamics from NMR diffusion measurements. Ch. 11 in *Asphaltenes, Heavy Oils and Petroleomics*; Mullins, O. C., Sheu, E. Y., Hammami, A., Marshall, A. G., Eds.; Springer: New York, 2007.

(7) Andrews, A. B.; Guerra, R.; Sen, P. N.; Mullins, O. C. *J. Phys. Chem. A* **2006**, *110*, 8095.

(8) Schneider, M. H.; Andrews, A. B.; Mitra-Kirtley, S.; Mullins, O. C. Asphaltene Molecular Size by Fluorescence Correlation Spectroscopy. *Energy Fuels* **2007**, *21* (5), 2875–2882.

(9) Guerra, R.; Andrews, A. B.; Mullins, O. C.; Sen, P. N. Comparison of asphaltene molecular diffusivity of various asphaltenes by fluorescence correlation spectroscopy. *Fuel* **2007**, *86*, 2016–2020.

(10) Boduszynski, M. M. Ch. 7 in *Chemistry of Asphaltenes*; Bunger, J. W., Li, N.C., Eds.; American Chemical Society: Washington, DC, 1981.

(11) Zhan, D.; Fenn, J. B. Electrospray mass spectrometry of fossil fuels. *Int. J. Mass Spectrom.* **2000**, *194*, 197–208.

(12) Rodgers, R. P.; Marshall, A. G. Petroleomics: Advanced Characterization of Petroleum Derived Materials by Fourier Transform Ion Cyclotron Resonance Mass Spectrometry (FT-ICR MS). Ch. 3 in *Asphaltenes, Heavy Oils and Petroleomics*; Mullins, O. C., Sheu, E. Y., Hammami, A., Marshall, A. G., Eds.; Springer: New York, 2007

(13) Klein, G. C.; Kim, S.; Rodgers, R. P.; Marshall, A. G.; Yen, A.; Asomaning, S. Mass Spectral Analysis of Asphaltenes. I. Compositional Differences between Pressure-Drop and Solvent-Drop Asphaltenes Determined by Electrospray Ionization Fourier Transform Ion Cyclotron Resonance Mass Spectrometry. *Energy Fuels* **2006**, *20*, 1965–1972.

(14) Martinez-Haya, B.; Hortal, A. R.; Hurtado, P. M.; Mullins, O. C. Molecular weight distributions of coal and petroleum asphaltenes from laser desorption ionization experiments. *Energy Fuels* **2007**, *21*, 2863–2868.

(15) Pomerantz, A. E.; Hammond, M. R.; Morrow, A. L.; Mullins, O. C.; Zare, R. N. Two-Step Laser Mass Spectrometry of Asphaltenes. *J. Am. Chem. Soc.* **2008**, *130*, 7216–7217.

(16) Pomerantz, A. E.; Hammond, M. R.; Morrow, A. L.; Mullins, O. C.; Zare, R. N. Asphaltene Molecular Weight Distribution Determined by Two-Step Laser Mass Spectrometry. *Energy Fuels* **2009**, *23*, 1162–1168.

(17) Sabbah, H; Morrow, A. L.; Pomerantz, A. E.; Zare, R. N. Evidence for island structures as the dominant architecture of asphaltenes. *Energy Fuels* **2011**, *25*, 1597–1604.

(18) Rodgers, R. P.; Tan, X.; Ehrmann, B. M.; Juyal, P.; McKenna, A. M.; Purcell, J. M.; Schaub, T. M.; Gray, M. R.; Marshall, A. G. Asphaltene Structure Determined by Mass Spectrometry. 9th International Conference on Petroleum Phase Behavior & Fouling, Victoria, B. C., Canada, 15−19 June, 2008; Abstract 102.

(19) Borton, D., II; Pinkston, D. S.; Hurt, M. R.; Tan, X.; Azyat, K.; Tykwinski, R.; Gray, M.; Qian, K.; Kenttämaa, H. I. Molecular Structures of Asphaltenes Based on the Dissociation Reactions of Their Ions in Mass Spectrometry. *Energy Fuels* **2010**, *24*, 5548–5559.

(20) Ruiz-Morales, Y.; Mullins, O. C. Polycyclic Aromatic Hydrocarbons of Asphaltenes Analyzed by Molecular orbital Calculations with Optical Spectroscopy. *Energy Fuels* **2007**, *21*, 256.

(21) Andrews, A. B.; McClelland, A.; Korkeila, O.; Demidov, A.; Krummel, A.; Mullins, O. C.; Chen, Z. Molecular Orientation of Asphaltenes and PAH Model Compounds in Langmuir-Blodgett Films Using Sum Frequency Generation Spectroscopy. *Langmuir* **2011**, *27* (10), 6049–6058.

(22) Buch, L; Groenzin, H; Buenrostro-Gonzalez, E; Andersen, S. I.; Lira-Galeana, C; Mullins, O. C. Effect of hydrotreatment on asphaltene fractions. *Fuel* **2003**, *82*, 1075–84.

(23) Solum, M. S.; Pugmire, R. J.; Grant, D. M. ^{13}C Solid-State NMR of Argonne Premium Coals. *Energy Fuels* **1989**, *3*, 187–193.

(24) Solum, M. S.; Sarofim, A. F.; Pugmire, R. J.; Fletcher, T. H.; Zhang, H. ^{13}C NMR Analysis of Soot Produced from Model Compounds and a Coal. *Energy Fuels* **2001**, *15*, 961–971.

(25) Pugmire, R. J.; Solum, M. S.; Grant, D. M.; Critchfield, S.; Fletcher, T. H. Structural Evolution of Matched Tar-Char Pairs in Rapid Pyrolysis Experiments. *Fuel* **1991**, *70*, 414.

(26) Siskin, M.; Kelemen, S. R.; Eppig, C. P.; Brown, L. D.; Afeworki, M. Asphaltene Molecular Structure and Chemical Influences on the Morphology of Coke Produced in Delayed Coking. *Energy Fuels* **2006**, *20*, 1227–1234.

(27) Kelemen, S. R.; Afeworki, M.; Gorbaty, M. L.; Sansone, M.; Kwiatek, P. J.; Walters, C. C.; Freund, H.; Siskin, M.; Bence, A. E.; Curry, D. J.; Solum, M.; Pugmire; Vandenbroucke, R. J. M.; Leblond, M.; Behar, F. Direct Characterization of Kerogen by X-Ray and Solid-State ^{13}C Nuclear Magnetic Resonance Methods. *Energy Fuels* **2007**, *21*, 1548–1561.

(28) Fletcher, T. H.; Kerstein, A. R.; Pugmire, R. J.; Solum, M. S.; Grant, D. M. Chemical Percolation Model for Devolatilization. 3. Direct Use of ^{13}C NMR Data to Predict Effects of Coal Type. *Energy Fuels* **1992**, *6*, 414–431.

(29) Sheremata, J. M.; Gray, M. R.; Dettman, H. D.; McCaffrey, W. C. Quantitative Molecular Representation and Sequential Optimization of Athabasca Asphaltenes. *Energy Fuels* **2004**, *18*, 1377–1384.

(30) Michon, L.; Martin, D.; Planche, J.-P.; Hanquet, B. Estimation of average molecule parameters of bitumens by ^{13}C nuclear magnetic resonance spectroscopy. *Fuel* **1997**, *76*, 9–15.

(31) Japanwala, S.; Chung, K. H.; Dettman, H. D.; Gray, M. R. Quality of Distillates from Repeated Recycle of Residue. *Energy Fuels* **2002**, *16*, 477–484.

(32) Christopher, J.; Sarpal, A. S.; Kapur, G. S.; Krishna, A.; Tyagi, B. R.; Jain, M. C.; Jain, S. K.; Bhatnagar, A. K. Chemical Structure of Bitumen-Derived Asphaltenes by Nuclear Magnetic Resonance Spectroscopy and X-Ray Diffractometry. *Fuel* **1996**, *75*, 999–1008.

(33) Hirano, K. Outline of NEDOL coal liquefaction process development (pilot plant program). *Fuel Process. Technol.* **2000**, *62* (2−3), 109–118.

(34) Ikeda, K.; Sakawaki, K.; Nogami, Y.; et al. Kinetic evaluation of progress in coal liquefaction in the 1 t/d PSU for the NEDOL process. *Fuel* **2000**, *79* (3−4), 373–378.

(35) Boduszynski, M. M.; Altgelt, K. H. *Composition and Analysis of Heavy Petroleum Fractions*; Marcel Dekker: New York, 1994.

(36) Bartle, K. D.; Ladner, W. R.; Martin, T. G.; Snape, C. E.; Williams, D. F. Structural Analysis of supercritical gas extracts of coals. *Fuel* **1979**, *58*, 413–422.

(37) Maekawa, Y.; Yoshida, T.; Yoshida, Y. Quantitative ^{13}C NMR Spectroscopy of a coal derived oil and the assignment of chemical shifts. *Fuel* **1979**, *58*, 864–972.

(38) Abu-Dagga, F.; Ruegger, H. Evaluation of low boiling crude oil fractions by NMR spectroscopy. Average Structural Parameters and identification of aromatic components by 2D NMR Specroscopy. *Fuel* **1988**, *67*, 1255–1262.

(39) Friebolin, H. *Basic One- and Two-Dimensional NMR Spectroscopy*; Wiley-VCH, 1991; pp 192−197.

(40) Netzel, D. A. Quantification of carbon types using DEPT/QUAT NMR pulse sequences: Application to fossil fuel derived oils. *Anal. Chem.* **1987**, *59*, 1775.

(41) Netzel, D. A.; Guffey, E. D. NMR and GC/MS Investigation of the Saturate Fraction from the Cerro Negro Heavy Petroleum Crude. *Energy Fuels* **1989**, *3*, 455–460.

(42) Behera, B.; Ray, S. S.; Singh, I. D. Structural Characterization of FCC Feeds from Indian Refineries by NMR Spectroscopy. *Fuel* **2008**, *87*, 2322–2333.

(43) Cookson, D. J.; Smith, B. E. Quantitative Estimation of CHn Group Abundances in Fossil Fuel Materials using ^{13}C NMR Methods. *Fuel* **1983**, *62*, 986–988.

(44) Dereppe, J. M.; Moreux, C. Measurement of CH_n Group Abundances in Fossil Fuel Materials using DEPT ^{13}C NMR. *Fuel* **1985**, *64*, 1174–1176.

(45) Jiang, B.; Xiao, N.; Liu, H.; Zhou, Z.; Mao, X. A.; Liu, M. Optimized Quantitative DEPT and Quantitative POMMIE Experiments for ^{13}C NMR. *Anal. Chem.* **2008**, *80*, 8293–8298.

(46) Montanari, L.; Montani, E.; Corno, C.; Fattori, S. NMR Molecular Characterization of Lubricating Base Oils: Correlation with Their Performance. *Appl. Magn. Reson.* **1998**, *14*, 345–356.

(47) Diaz, C.; Blanco, C. G. NMR: A Powerful Tool in the Characterization of Coal tar Pitch. *Energy Fuels* **2003**, *17*, 907–913.

(48) Morgan, T. J.; George, A.; Davis, D. B.; Herod, A. A.; Kandiyoti, R. Optimization of ^{1}H and ^{13}C NMR Methods for Structural Characterization of Acetone and Pyridine Soluble Fractions of a Coal tar Pitch. *Energy Fuels* **2008**, *22*, 1824–1835.

(49) Masuda, K.; Okuma, O.; Nishizawa, T.; Kanaji, M.; Matsumura, T. High Temperature NMR Analysis of Aromatic Units in Asphaltenes and Preasphaltenes Derived from Victorian Brown Coal. *Fuel* **1996**, *75*, 295–299.

(50) Begon, V.; Suelves, I.; Islas, C. A.; Millan, M.; Dubau, C.; Lazaro, M.-J.; Law, R. V.; Herod, A. A.; Dugwell, D. R.; Kandiyoti, R. Comparison of Quaternary Aromatic Carbon Contents of a Coal, a Coal Extract, and its Hydrocracking Products by NMR Methods. *Energy Fuels* **2003**, *17*, 1616–1629.

(51) Bergmann, U.; Groenzin, H.; Mullins, O. C.; Glatzel, P.; Fetzer, J.; Cramer, S. P. Carbon K-edge X-ray Raman spectroscopy supports simple, yet powerful description of aromatic hydrocarbons and asphaltenes. *Chem. Phys. Lett.* **2003**, *369*, 184–191.

(52) Bergmann, U.; Glatzel, P.; Cramer, S. P. Bulk-sensitive XAS characterization of light elements: from X-ray Raman scattering to X-ray Raman spectroscopy. *Microchem. J.* **2002**, *71*, 221–230.

(53) Waber, J. T.; Cromer, D. T. Orbital Radii of Atoms and Ions. *J. Chem. Phys.* **1965**, *42*, 4116–4123.

(54) Stöhr, J. *NEXAFS Spectroscopy*; Springer: Berlin, 1992; p 403.

(55) Sharma, A.; Groenzin, H.; Mullins, O. C.; Tomita, A. Probing order in asphaltenes and aromatic ring systems by HRTEM. *Energy Fuels* **2002**, *16* (2), 490.

(56) Bergmann, U.; Groenzin, H.; Mullins, O. C.; Glatzel, P.; Fetzer, J.; Cramer, S. P. X-Ray Raman Spectroscopy--A New Tool to Study Local Structure of Aromatic Hydrocarbons and Asphaltenes. *Pet. Sci. Technol.* **2004**, *22*, 863–875.

(57) Clar, E. *The Aromatic Sextet*; John Wiley & Sons: London, 1972; p 128.

(58) Gould, K. A.; Wiehe, I. A. Natural Hydrogen Donors in Petroleum Resids. *Energy Fuels* **2007**, *21*, 1199–1204.

(59) Artok, L.; Su, Y.; Hirose, Y.; Hosokawa, M.; Murata, S.; Nomura, M. Structure and Reactivity of Petroleum-Derived Asphaltenes. *Energy Fuels* **1999**, *13*, 287–296.

(60) Sharma, B. K.; Adhvaryu, A.; Perez, J. M.; Erhan, S. Z. Effects of hydro-processing on structure and properties of base oils using NMR. *Fuel Proc. Technol.* **2008**, *89*, 984.

(61) Mojelsky, T. W.; Ignasiak, T. M.; Frackman, Z.; McIntyre, D. D.; Lown, E. M.; Montgomery, D. S.; Strausz, O. P. Structural Features of Alberta Oil Sand Bitumen and Heavy Oil Asphaltenes. *Energy Fuels* **1992**, *6*, 83–96.

(62) Su, Y.; Artok, L.; Murata, S.; Nomura, M. Structual Analysis of the Asphaltene Fraction of an Arabian Mixture by a Ruthenium-Ion-Catalyzed Oxidation Reaction. *Energy Fuels* **1998**, *12*, 1265–1271.

(63) Strausz, O. P.; Mojelsky, T. W.; Faraji, F.; Lown, E. M.; Peng, P. a. Additional Structural Details on Athabasca Asphaltene and Their Ramifications. *Energy Fuels* **1999**, *13*, 207–227.

(64) Lehne, E.; Dieckmann, V. Improved understanding of mixed oil in Nigeria based on pyrolysis of asphaltenes. *Org. Geochem.* **2010**, *41*, 661–674.

(65) Cyr, N.; McIntyre, D. D.; Toth, G.; Strausz, O. P. Hydrocarbon structural group analysis of Athabsca asphaltene and its g.p.c. fractions by ^{13}C NMR. *Fuel* **1987**, *66*, 1709–1714.

(66) Dittmar, T.; Koch, B. P. Thermogenic organic matter dissolved in the abyssal ocean. *Mar. Chem.* **2006**, *102*, 208–217.